molecular pharmaceutics

ARTICLE

pubs.acs.org/molecularpharmaceutics

Thermodynamic and Structural Aspects of Novel 1,2,4-Thiadiazoles in Solid and Biological Mediums

German L. Perlovich,*[,†,‡] Alexey N. Proshin,[‡] Tatyana V. Volkova,[†] Cong Trinh Bui,[†] and Sergey O. Bachurin[‡]

[†]Institute of Solution Chemistry, Russian Academy of Sciences, 153045 Ivanovo, Russia

[‡]Institute of Physiologically Active Compounds, Russian Academy of Sciences, 142432, Chernogolovka, Russia

ABSTRACT: Novel 1,2,4-thiadiazoles were synthesized. Crystal structures of these compounds were solved by X-ray diffraction experiments, and comparative analysis of packing architecture and hydrogen bond networks was carried out. Thermodynamic aspects of sublimation processes of the compounds under study were analyzed using temperature dependencies of vapor pressure. Thermophysical characteristics of the molecular crystals were obtained and compared with the sublimation and structural parameters. The melting points correlate with sublimation Gibbs energies. Moreover, an increase of donor−acceptor interactions in crystal structures leads to growth of Gibbs energy values. Relationships between the melting points and the fragmental contributions to the packing energies were established: R_1-R_4 fragmental interactions are responsible for the fusion processes of this class of compounds. Solubility and solvation processes of 1,2,4-thiadiazoles in buffer, *n*-hexane and *n*-octanol were studied within a wide range of temperature intervals, and their thermodynamic functions were calculated. Specific and nonspecific interactions of molecules resolved in crystals and solvents were estimated and compared. It was found that the melting points correlate with sublimation Gibbs energies. Distribution processes of compounds in buffer/*n*-octanol and buffer/*n*-hexane systems (describing different types of membranes) were investigated. Transfer processes of the studied molecules from the buffer to *n*-octanol/*n*-hexane phases were analyzed by the diagram method with evaluation of the enthalpic and entropic terms. This approach allowed us to design drug molecules with optimal passive transport properties. Calcium-blocking properties of the substances were evaluated. The trend between the ability to inhibit Glu-Ca uptake and the distribution coefficients in buffer/hexane system was observed.

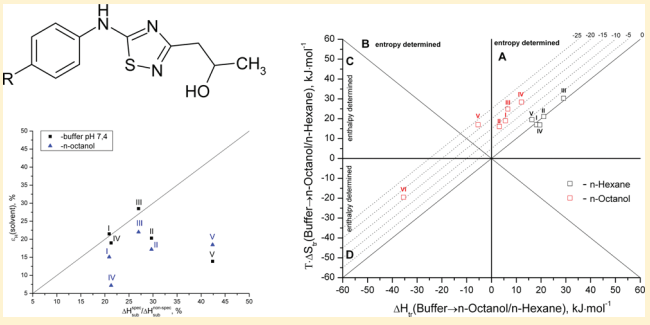

KEYWORDS: 1,2,4-thiadiazoles, sublimation thermodynamics, solubility, solvation, crystal structure, transfer process, distribution

1. INTRODUCTION

One of the principal disorders of the central nervous system is Alzheimer's disease (AD). The biological mechanism underlying the development of AD is complex, as several factors contribute to the neuropathology of the disease. Thiadiazole related compounds have been successfully described as potential drugs for treatment of AD.[1−6] Interaction of the drug molecule with target receptors is a key feature in designing of drug molecules. Nevertheless, effectiveness of drug substances is dependent on their concentration level at the receptor and determined by drug delivery processes. Therefore, screening parameters characterizing the solubility, partitioning and passive transport processes is an essential part of the drug design.

Hansch's group[7] suggested that the octanol−water partitioning (log P_{oct}) is the most commonly used method in QSAR studies. The property value of about 2 represents the optimal lipophilic nature of the tested molecule which is required for penetrating the central nervous system (CNS); however, this rule is not based on the permeability rates or equilibrium concentrations, instead, it only takes into account biological activity tests. Two decades ago Young et al.[8] failed to predict the brain penetration of H2 antagonists. The log *P* data from the cyclohexane−water system (log P_{chex}) were likewise inadequate. In contrast, Young et al.[8] reported that there is a significant correlation between the difference of log P_{oct} and log P_{chex} data (Δlog *P*), on the one hand, and the logarithm of the brain/blood equilibrium concentration ratios of H2 antagonists, on the other hand. They concluded that Δlog *P* accounts for hydrogen bonding and reflects two different processes. The log P_{chex} value quantifies the partitioning of the molecule into nonpolar regions of the brain, whereas the log P_{oct} value describes protein interactions in blood. Thus, in order to optimize the brain penetration of a drug molecule the overall H-bonding property of this molecule has to be minimized. Abraham and colleagues[9−11] suggest that not only is the hydrogen bond acidity important but also the solute hydrogen

Received: April 2, 2011
Accepted: July 29, 2011
Revised: July 18, 2011
Published: July 29, 2011

dx.doi.org/10.1021/mp2003237 | *Mol. Pharmaceutics* 2011, 8, 1807–1820

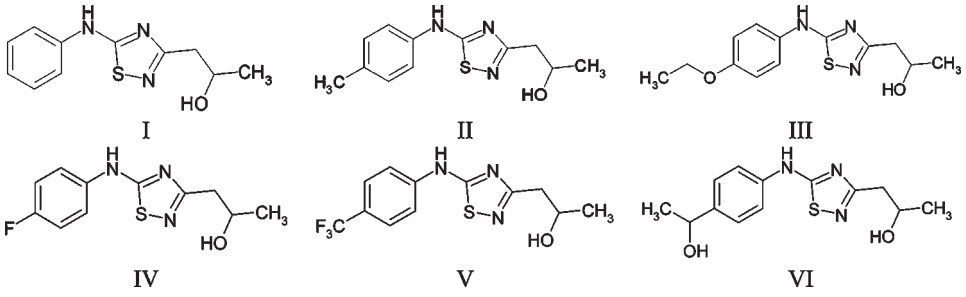

Figure 1. Molecular structure of the studied compounds.

bond basicity and dipolarity/polarizability contribute and lead to a more negative $\Delta\log P$ value, thus favoring the penetration through the blood−brain barrier. In other words, the larger the solute, the more negative the $\Delta\log P$ value becomes, thereby favoring penetration into the brain.

This work is a continuation of our previous study of 1,2,4-thiadiazole derivatives with different substitution groups in the para position: H−, **I**; CH_3−, **II**; and C_2H_5O−, **III** (Figure 1).[12] In order to analyze the influence of substituents on physicochemical properties of the compounds in solids and solutions, the set of substances was expanded, and the novel substitution groups are follows: F−, **IV**; CF_3−, **V**; and CH_3OHCH−, **VI** (Figure 1). We chose these objects for a number of reasons. On the one hand, our laboratory is focused on studying the effects of such compounds on the biological activity of certain receptors that are involved in AD pathology. On the other hand, the delivery of thiadiazoles to their target organs is poorly understood. In our opinion, investigation of the selected compounds using a wide spectrum of experimental methods (X-ray diffraction experiment, isothermal saturation method, transpiration method, differential scanning calorimetry) makes it possible not only to understand drug transport and delivery processes but also to find out regularities for prediction of the required pharmacological and pharmaceutical characteristics.

2. MATERIAL AND METHODS

2.1. Compounds and Solvents. 1-Octanol (*n*-octanol, $CH_3(CH_2)_7OH$, MW 130.2, lot 11K3688) ARG was received from Sigma Chemical Co. (USA). *n*-Hexane (C_6H_{14}, MW 86.18, lot TU 2631-006-29483781-2008) ARG was received from Kchimmed (Moscow, Russia). The buffer solutions pH 7.4 were prepared by mixing solutions of appropriate sodium and potassium salts of phosphoric acid, manufactured in Kchimmed (Moscow, Russia), as described elsewhere.[13] Ionic strength was adjusted by adding potassium chloride. All chemicals were of AR grade. The pH values were measured by using and electroanalytical analyzer, type OP-300, Radelkis, Budapest, standardized with pH 1.68, 6.86, and 9.22 solutions.

2.2. Single Crystal Preparation. Single crystals of compound **IV** were grown by slow evaporation of methanol from the corresponding solution for 7 days. Single crystals of compound **V** were prepared by slow evaporation of 1,4-dioxane from the corresponding solution for 21 days. Finally, single crystals of compound **VI** were grown by slow evaporation of methanol from the corresponding solution for 10 days.

2.3. X-ray Diffraction Experiments. Single-crystal X-ray measurements were carried out using a Nonius CAD-4 diffractometer (Netherlands) with graphite-monochromated Mo K_α radiation (λ = 0.71069 Å). The intensity data were collected at 25 °C by means of a $\omega-2\theta$ scanning procedure. The crystal structures were solved using direct methods and refined by means of a full-matrix least-squares procedure. *CAD-4* Software[14] was applied for data collection, data reduction and cell refinement. *SHELXS-97* and *SHELXL-97* software programs[15] were used to solve and to refine structures, respectively.

2.4. Solubility Determination. All the experiments were carried out by the isothermal saturation method at several temperature points: 20, 25, 30, 37, 42 ± 0.1 °C. All experimental data has been presented/recalculated in molar fraction units. The solid phase was removed by isothermal filtration (Acrodisc CR syringe filter, PTFE, 0.2 μm pore size, Carrigiwohill, Co. Cork, Ireland) or centrifugation (Biofuge pico, Thermo Electron LED GmbH, Germany) at 2000 rpm for 5 min. The experimental results are reported as an average value of at least three replicated experiments. The molar solubilities of drugs were measured spectrophotometrically with an accuracy of 2−2.5% using a protocol described previously.[16]

The standard Gibbs energies of dissolution processes ΔG°_{sol} (in $kJ\cdot mol^{-1}$) were calculated using the following equation:

$$\Delta G^\circ_{sol} = -RT \ln a_2 \quad (1)$$

where $a_2 = \gamma_2 \cdot X_2$ is the activity of the solute molecule; X_2 is the drug molar fraction in the saturated solution; γ_2 is the activity coefficient of the solute molecule. The standard solution enthalpies ΔH°_{sol} (in $kJ\cdot mol^{-1}$) were calculated using the van't Hoff equation:

$$\partial(\ln a_2)/\partial T = \Delta H^\circ_{sol}/RT^2 \quad (2)$$

The activity coefficients were estimated from the concentration dependencies of buffer−*n*-octanol distribution of the compounds studied at 25 °C. It was assumed that the solution enthalpies are independent of the concentration. The temperature dependencies of drug solubilities within the chosen temperature interval can be described by the linear function

$$\ln X_2 = A - B/T \quad (3)$$

where A = integral coefficient relating to enthropy; $B = \Delta H^\circ_{sol}/R$.

This indicates that the change in heat capacity of the solutions with the temperature is negligibly small.

The standard solution entropies ΔS°_{sol} (in $J\cdot mol^{-1}\cdot K^{-1}$) were obtained from the well-known equation

$$\Delta G^\circ_{sol} = \Delta H^\circ_{sol} - T\Delta S^\circ_{sol} \quad (4)$$

2.5. Distribution Experiments. The distribution coefficients of buffer−*n*-octanol ($D^{7.4\rightarrow oct}$) were determined by the

isothermal saturation method. The procedure was as follows: in an ampule placed inside a thermostat we put a definite volume of a buffer saturated *n*-octanol solution with a certain concentration of the compound under study and an identical volume of octanol saturated buffer. The experiment lasted over two days with the ampule continuously shaken. By applying UV spectrophotometry we determined the drug concentration after the distribution in the octanol-saturated buffer phase (C_2^{bo}), the initial concentration in the buffer-saturated octanol phase ($C_2^{ob}(i)$), and the final concentration of the substance in the buffer-saturated octanol phase ($C_2^{ob}(f)$). The distribution coefficient was calculated by

$$D^{7.4 \rightarrow oct} = C_2^{ob}(f)/C_2^{bo} \quad (5)$$

The accuracy of the $D^{7.4 \rightarrow oct}$ value was verified by checking the mass balance of the starting amount of the compound compared to the total amount of the compound distributed between the two phases,

$$n_2^{ob}(i) = n_2^{ob}(f) + n_2^{bo} \quad (6)$$

where $n_2^{ob}(i) = C_2^{ob}(i) \cdot V^{ob}$ and $n_2^{ob}(f) = C_2^{ob}(f) \cdot V^{ob}$ are the number of moles of the solute in the initial and in the final octanol phase, respectively. $C_2^{ob}(i)$ and $C_2^{ob}(f)$ are the molar concentrations of the solute in the buffer-saturated octanol, before (i) and after (f) the experiment, respectively. V^{ob} is the volume of the octanol phase. $n_2^{ob} = C_2^{ob} \cdot V^{ob}$ is the number of solute moles in the octanol-saturated buffer. Each experiment was repeated at least three times.

The distribution coefficient of the compounds studied in the buffer−*n*-hexane phase ($D^{7.4 \rightarrow hex}$) was determined in the same way as for the buffer−*n*-octanol phase. As the tested compounds are weakly soluble in the *n*-hexane, the initial and final concentrations were measured for the buffer solution.

2.6. Estimation of Activity Coefficients of Compounds in *n*-Octanol Phase. The activity coefficient of the studied compounds was estimated by the concentration dependencies of the distribution coefficients using the following procedure:

$$D_{c(max)}^{7.4 \rightarrow oct} = a_2^{ob}(C_{max})/a_2^{bo}(C_{max}) \quad (7)$$

$$D_{c(min)}^{7.4 \rightarrow oct} = a_2^{ob}(C_{min})/a_2^{bo}(C_{min}) \quad (8)$$

where $D_{c(max)}^{7.4 \rightarrow oct}$ is the distribution coefficient at the maximum concentration of the solute in the octanolic phase whereas $D_{c(min)}^{7.4 \rightarrow oct}$ is the distribution coefficient at the minimal concentration of the solute in the octanolic phase.

$$D_{c(max)}^{7.4 \rightarrow oct}/D_{c(min)}^{7.4 \rightarrow oct} = (a_2^{ob}(C_{max})/a_2^{ob}(C_{min}))/(a_2^{bo}(C_{max})/a_2^{bo}(C_{min})) = \gamma_2^{ob}/\gamma_2^{bo} \quad (9)$$

If we take into account the low solubility of the substances studied in the buffer phase, we can assume that $\gamma_2^{bo} \approx 1$.

$$\gamma_2^{o} \approx \gamma_2^{ob} \approx D_{c(max)}^{7.4 \rightarrow oct}/D_{c(min)}^{7.4 \rightarrow oct} \quad (10)$$

2.7. Sublimation Experiments. Sublimation experiments were carried out by the transpiration method described elsewhere.[17] In brief, a stream of an inert gas passes above the sample at a constant temperature and at known slow constant flow rate in order to achieve saturation of the carrier gas with the vapor of the compound being tested. The vapor is condensed at some point downstream, and the mass of sublimate and its purity are determined. The vapor pressure over the sample at this temperature is calculated by the amount of the sublimated sample and the volume of the inert gas used.

The equipment was calibrated using benzoic acid. The standard value of sublimation enthalpy obtained here was $\Delta H_{sub}^{\circ} = 90.5 \pm 0.3$ kJ·mol^{-1}. This is in good agreement with the value recommended by IUPAC of $\Delta H_{sub}^{\circ} = 89.7 \pm 0.5$ kJ·mol^{-1}.[18] The saturated vapor pressures were measured at each temperature five times with the standard deviation being within 3−5%. Since the saturated vapor pressure of the tested compounds is low, it may be assumed that the heat capacity change of the vapor with temperature is negligibly small. The experimentally determined vapor pressure data may be described in (ln P; $1/T$) coordinates in the following way:

$$\ln(P) = A + B/T \quad (11)$$

The value of the sublimation enthalpy is calculated by the Clausius−Clapeyron equation:

$$\Delta H_{sub}^{T} = RT^2 \cdot \partial(\ln P)/\partial(T) \quad (12)$$

whereas the sublimation entropy at a given temperature T was calculated by the following relation:

$$\Delta S_{sub}^{T} = (\Delta H_{sub}^{T} - \Delta G_{sub}^{T})T \quad (13)$$

with $\Delta G_{sub}^{T} = -RT \cdot \ln(P/P_0)$, where $P_0 = 10^5$ Pa.

Sublimation data are yielded at elevated temperatures for experimental reasons. However, in comparison with effusion methods the temperatures in our case are much lower, which makes the extrapolation to room temperature conditions easier. In order to further improve the extrapolation to room conditions, heat capacities ($C_{p,cr}^{298}$ value) of the crystals were estimated using the additive scheme proposed by Chickos et al.[19] Heat capacity was introduced as a correction for the recalculation of the sublimation enthalpy ΔH_{sub}^{T} value at 298 K (ΔH_{sub}^{298} value) according to the equation[19]

$$\Delta H_{sub}^{298} = \Delta H_{sub}^{T} + \Delta H_{cor} = \Delta H_{sub}^{T} + (0.75 + 0.15C_{p,cr}^{298}) \cdot (T - 298.15) \quad (14)$$

2.8. Differential Scanning Calorimetry. Differential scanning calorimetry (DSC) was carried out using a DSC 204 F1 "Foenix" (Netzsch, Germany). DSC runs were performed in the atmosphere of flowing (25 mL·min^{-1}) dry argon gas of high purity 99.996% using standard aluminum sample pans and a heating rate of 10 K·min^{-1}. The DSC was calibrated using five standards: Hg, biphenyl, indium, tin and bismuth. The sample mass was in the range of 1−5.5 mg, determined with the accuracy of ±0.005 mg using the balance Sartorius M2P. The experiment was repeated twice.

2.9. Calculation Procedure. The free volume in the crystal lattice was estimated on the basis of the X-ray diffraction data and van der Waals molecular volume (V^{vdw}), calculated by GEPOL:[20]

$$V^{free} = (V_{cell} - Z \cdot V^{vdw})/Z \quad (15)$$

where V_{cell} is the volume of the unit cell and Z is the number of molecules in the unit cell.

The parameter $\beta = V^{free}/V^{vdw}$ has been introduced for the description of the packing density of molecules in the crystal. It is

Table 1. Crystal Lattice Parameters of the Substances under Investigation[a]

	IV	V	VI
crystal system	monoclinic	orthorhombic	monoclinic
space group	$P2_1/c$	$Pbca$	$P2_1/c$
crystal size, mm	0.2 × 0.2 × 0.2	0.15 × 0.15 × 0.15	0.2 × 0.2 × 0.2
a, Å	7.6540(15)	11.266(2)	8.122(4)
b, Å	18.156(4)	10.914(2)	8.467(4)
c, Å	9.2820(19)	23.160(5)	20.481(8)
β, deg	113.94(3)	90.00	90.70(3)
volume, Å^3	1178.9(4)	2847.7(10)	1408.4(11)
Z	4	8	4
D_{calc}, g·cm^{-3}	1.427	1.415	1.318
radiation	Mo K$_\alpha$	Mo K$_\alpha$	Mo K$_\alpha$
T, K	293(2)	293(2)	293(2)
μ, mm^{-1}	0.274	0.259	0.232
data collection			
measd reflns	2692	2098	2973
indep reflns	2343	1570	2770
indep reflns with >2$\sigma(I)$	721	395	650
θ_{max}, deg	26	25	26
refinement			
refinement on	F^2	F^2	F^2
$R[F^2 > 2\sigma(F^2)]$	0.0777	0.0880	0.0688
$\omega R(F^2)$	0.1859	0.1101	0.1299
S	0.992	1.061	0.979
reflns	2343	1570	2770
parameters	156	179	175
$(\Delta/\sigma)_{max}$	0.000	0.001	0.001
$\Delta\rho_{max}$, e·Å^{-3}	0.338	0.247	0.445
$\Delta\rho_{min}$, e·Å^{-3}	−0.417	−0.211	−0.345
V^{vdw}, Å^3	199.8	223.7	236.1
V_{mol},[b] Å^3	294.7	356.0	352.1
V^{free},[c] Å^3	94.9	132.3	116
V^{free}/V^{vdw}, %	47.5	59.1	49.1

[a] The standard deviations are displayed within parentheses. [b] $V_{mol} = V_{cell}/Z$. [c] $V^{free} = (V_{cell} - Z \cdot V^{vdw})/Z$

inversely proportional to the packing density and shows the change of the free volume falling on one molecule in the crystal, with increasing of it is van der Waals volume.

All descriptors were calculated by the program package HYBOT-PLUS (version of 2003 year) in Windows.[21]

Nonbonded van der Waals interactions of crystal lattice energy were calculated as a sum of atom−atom interactions utilizing a Gavezzotti et al.[22] force field and cutoff radius of 16 Á. The hydrogen bonding energy was calculated using a Mayo et al.[23] force field:

$$E^{HB} = D_{HB} \cdot [5(R_{hb}/R_{DA})^{12} - 6(R_{hb}/R_{DA})^{10}] \cdot \cos^4(\theta_{DHA}) \quad (16)$$

where D_{HB} = 39.7 kJ·mol^{-1} is the depth of potential well of pair potential during creation of hydrogen bond of H_2O dimer; R_{hb} = 2.75 Å; R_{DA} and θ_{DHA} are the distance and the angle between donor and acceptors atoms.

2.10. Synthesis of Compounds. The synthesis of 1-[5-(4-fluoro-phenylamino)-[1,2,4]thiadiazol-3-yl]-propan-2-one was based on the method of Vivona et al.[24] and described by us earlier.[12]

*1-[5-(4-Fluoro-phenylamino)-[1,2,4]thiadiazol-3-yl]-propan-2-ol (**IV**).* The 1-[(5-(4-fluoro-phenylamino)-[1,2,4]thiadiazol-3-yl]-propan-2-one (10 mmol) was dissolved in 20 mL of methanol. $NaBH_4$ (15 mmol) was added portionwise to the mixture, which was stirred for 30 min, at the same time the hydrogen gassing was stopped. The solvent was removed until the resulted residue was dry and then taken up in dichloromethane/water. The organic layer was separated, dried (over Na_2SO_4) and filtered. The solvent was evaporated resulting in the product (2.08 g, 82%) with mp 103−105 °C.

^{1}H NMR [200 MHz, DMSO-d_6] δ: 1.18 (3H, d, J = 6.3 Hz, CH_3), 2.72 (1H, dd, J = 4.0, 14.2 Hz, CH), 2.85 (1H, dd, J = 7.0, 14.2 Hz, CH), 4.17 (1H, m, CH), 4.35 (1H, d, J = 4.4 Hz, OH), 7.06 (2H, t, J = 8.3 Hz, ArH), 7.55 (2H, ddd, J = 2.38, 4.6, 9.1 Hz, ArH), 10.69 (1H, s, NH). Anal. ($C_{11}H_{12}FN_3OS$) C, H, N.

*1-[(5-(4-Trifluoromethyl-phenylamino)-[1,2,4]thiadiazol-3-yl]-propan-2-ol (**V**).* Compound **V** was obtained in a similar way from the appropriate ketone.

Yield: 85%; mp 143−145 °C. ^{1}H NMR [200 MHz, $CDCl_3$] δ: 1.35 (3H, d, J = 6.3, CH_3), 2.91 (1H, dd, J = 8.6, 15.5 Hz, CH), 3.08 (1H, dd, J = 3.0, 15.5 Hz, CH), 3.80 (1H, br s, OH), 4.36 (1H, m, CH), 7.39 (2H, d, J = 8.6 Hz, ArH), 7.70 (2H, d, J = 8.6 Hz, ArH), 9.30 (1H, br s, NH). Anal. ($C_{12}H_{12}F_3N_3O_2S$) C, H, N.

*1-{5-[4-(1-Hydroxy-ethyl)-phenylamino]-[1,2,4]thiadiazol-3-yl}-propan-2-ol (**VI**).* Compound **VI** was synthesized from 1-[(5-(4-acetyl-phenylamino)-[1,2,4]thiadiazol-3-yl]-propan-2-one.

Yield: 64%; mp 144−146 °C. ^{1}H NMR [200 MHz, DMSO-d_6] δ: 1.14 (3H, d, J = 6.0 Hz, CH_3), 1.33 (3H, d, J = 6.5 Hz, CH_3), 2.66 (1H, dd, J = 6.1, 14.2 Hz, CH), 2.81 (1H, dd, J = 7.0, 14.2 Hz, CH), 4.13 (1H, m, CH), 4.42 (1H, d, J = 4.4 Hz, OH), 4.66 (1H, m, CH), 4.84 (1H, d, J = 4.0 Hz, OH), 7.27 (2H, d, J = 8.4 Hz, ArH), 7.38 (2H, d, J = 8.4 Hz, ArH), 10.66 (1H, s, NH). Anal. ($C_{13}H_{17}N_3O_2S$) C, H, N.

2.11. Calcium-Blocking Property Experiments. Interaction between the compounds and glutamate-dependent calcium uptake system was studied on newborn (8−11 days old) rat brain synaptosomal P_2-fraction isolated according to the following method. Synaptosomes were suspended in the incubation buffer A (132 mM NaCl, 5 mM KCl, 5 mM HEPES) pH 7.4 and stored at 0 °C during all experiments. Aliquots of synaptosomes (50 μL) were transposed to buffer A containing the testing compound and ^{45}Ca samples. Calcium ion uptake was stimulated by introducing 200 μM of glutamate solution. After 5 min of incubation at 37 °C the process was terminated by filtration on GF/B-filters. The sample was washed three times with cold buffer B (145 mM KCl, 10 mM TRIS, 5 mM Trilon B) followed by measurements of radioactivity with scintillator counter SL-4000 Intertechnic.

In preliminary experiments, all compounds were tested at concentration of 100 μM for their ability to inhibit the glutamate stimulated Ca^{2+} uptake (Glu-Ca uptake). If inhibition of the Glu-Ca uptake was 50% and more, then further studies were carried out to determine the concentration dependence of its inhibition and the corresponding value of K_I was measured according to the following equation:

$$K_I = K(43/21) = [(Ca_4 - Ca_3)/(Ca_2 - Ca_1)] \times 100\% \quad (17)$$

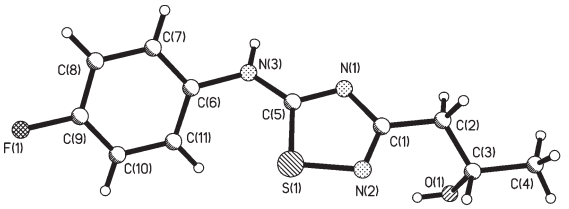

IV

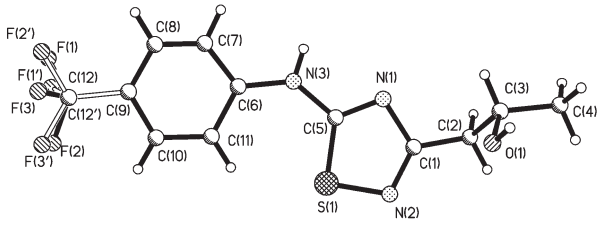

V

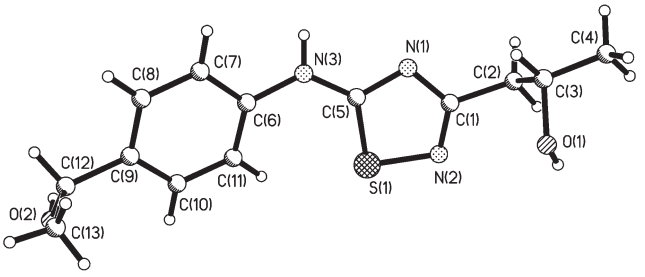

VI

Figure 2. View of the studied molecules with atomic numbering.

where Ca_1 is the Ca^{2+} influx in blank experiment (without glutamate and tested compounds); Ca_2 is the Ca^{2+} influx in the presence of glutamate only (Glu-Ca uptake); Ca_3 is the Ca^{2+} influx in the presence of tested compound (without glutamate); Ca_4 is the Ca^{2+} influx in the presence of both glutamate and tested compound.

3. RESULTS AND DISCUSSION

3.1. Crystal Structure Analysis. The results of the X-ray diffraction experiments are presented in Table 1. Views of the studied molecules with the atomic numbering are shown in Figure 2. It is evident that the CF_3- group of compound **V** in the crystal lattice is disordered, the probability between the two positions being 0.68 and 0.32.

The packing of molecules in the crystal lattices of the tested compounds is presented in Figure 3. For simplicity of analysis the disordered fragments are presented as atoms with the highest position probability. As Figure 3 shows, the molecular packing values in the crystals of the considered compounds differ essentially. Moreover, the number of hydrogen bonds per molecule and the hydrogen bond network topology change essentially as well. As an example of this, the geometric parameters of hydrogen bonds, graph set assignments for the two levels (using graph set notations terminology introduced by Etter[25] and revised by Bernstein[26]) are presented in Table 2. The

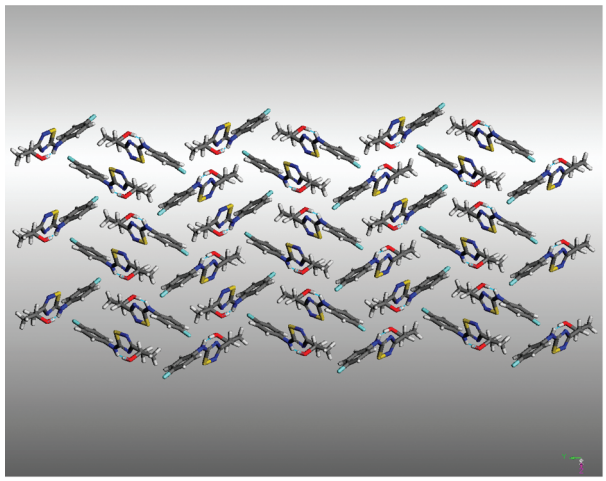

IV
a

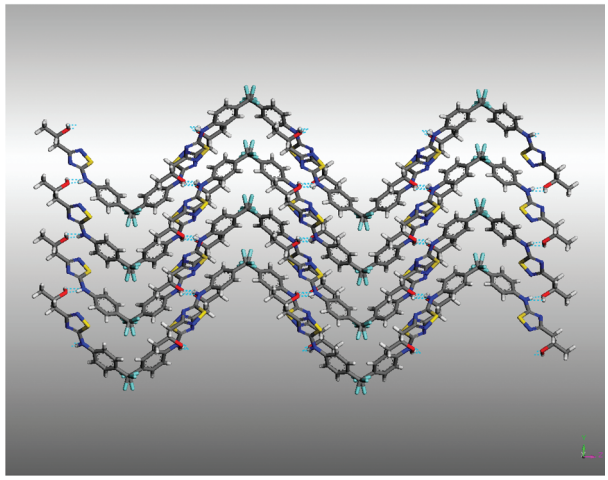

V
b

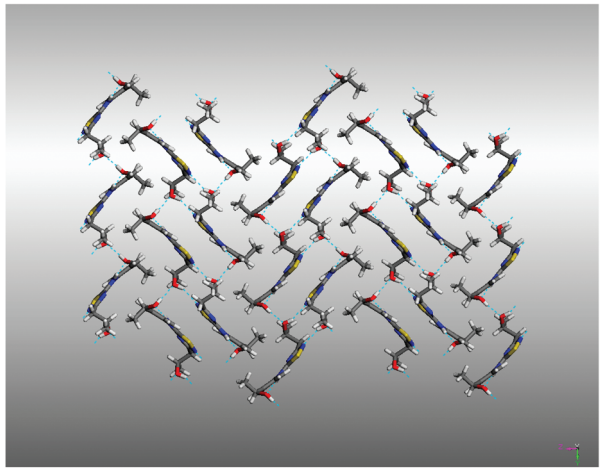

VI
c

Figure 3. Molecular packing architectures of crystal lattices of (a) **IV**, (b) **V** and (c) **VI** along the OX axis.

hydrogen bond energies, creating the diagonal elements of the graph set assignment matrixes by using Dreiding force field,[23] are

Table 2. Hydrogen Bond Geometry, Graph Set Notations and Hydrogen Bond Energies (E^{HB} in kJ·mol^{-1}) of the Diagonal Elements of the Graph Set Assignment Matrixes of Compounds IV–VI

IV	D–H···A[a]	D–H [Å]	H···A [Å]	D···A [Å]	D–H···A [deg]		a			$-E^{HB}$
a	N3–H3A···O1^{i}	0.860(19)	2.14(6)	2.88(5)	143(7)	a	C(8)			7.3
V	D–H···A[b]	D–H [Å]	H···A [Å]	D···A [Å]	D–H···A [deg]		a	b		$-E^{HB}$
a	N3–H3A···O1^{i}	0.860(31)	1.971(10)	2.811(11)	165(1)	a	C(8)			16.9
b	O1–H1B···N2^{ii}	0.820(47)	2.565(57)	3.359(86)	163(3)	b	$C_2^2(16)$	C(8)		5.9
VI	D–H···A[c]	D–H [Å]	H···A [Å]	D···A [Å]	D–H···A [deg]		a	b	c	$-E^{HB}$
a	O2–H2A···O1^{i}	0.819(64)	1.909(27)	2.720(29)	170(1)	a	C(14)			18.5
b	O1–H1A···N2^{ii}	0.819(73)	2.076(86)	2.825(05)	151(6)	b	$R_4^4(26)$	$R_2^2(12)$		11.2
c	N3–H3C···O2^{iii}	0.859(15)	2.016(70)	2.867(65)	170(5)	c	$C_2^2(10)$	$R_4^4(38)$	C(8)	17.2

[a] Symmetry code: (i) $x+1, y, z$. [b] Symmetry code: (i) $-x+1.5, y-1/2, z$; (ii) $-x+1.5, y+1/2, -z+1/2$. [c] Symmetry code: (i) $x-1, y+1, z$; (ii) $-x, -y+1, -z$; (iii) $x+1, y, z$.

Scheme 1

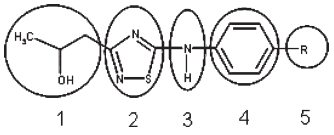

summarized in the same table. As it has been mentioned before, all the compounds have a different number of hydrogen bonds per molecule: **IV**, one; **V**, two; **VI**, three. The diagonal elements for **IV** and **V** are infinite chains with 8 involved atoms C(8). Moreover, the hydrogen bond energies of the two hydrogen bonds (a and b), forming the chain C(8) in **V**, differ from each other by approximately three times (Table 2). The substance **VI** has three diagonal elements: two infinite chains C(8) and C(14) with approximately equal hydrogen bond energies (17–18 kJ·mol^{-1}) and $R_2^2(12)$, describing dimer organization of the molecules in the crystals with hydrogen bond energy corresponding to 2/3 of the analogous bond in the chain.

In order to understand the influence of various molecular fragments on crystal lattice energy, we used the approach applied by us earlier.[27] The molecule was conditionally divided into a certain number of fragments, depending on the molecular topology. Segmentation for the five fragments (as a common case) is shown in Scheme 1. After that we calculated the contribution of the nonbonded van der Waals interactions to the packing energy from different fragment pairs of adjacent molecules. The results of the calculation for various energetic terms of the considered crystals are shown in Figure 4. The contributions of the fragments, creating intermolecular hydrogen bonds, are presented in the same figure (asterisks).

As Figure 4a shows, no regularity is observed between the fragment contributions to the packing energies of the various compounds. For example, the main contribution to the packing energy corresponds to the interaction between R_2 and R_4 fragments (i.e., interactions between phenyl and thiadiazole fragments): for substance **II**, R_4–R_4; for compound **III**, R_4–R_4 and R_1–R_2. For **IV** the dominant contributions are R_1–R_4 and R_1–R_2, whereas for **VI**, they are R_1–R_4. For the considered para-substituted compounds the contribution of R_4–R_4 interactions to the packing energy decreases if the molecular packing density falls (increase of $\beta = V^{free}/V^{vdw}$ parameter). For the substances with denser molecular packing we observed an essential difference of the values (4 kJ·mol^{-1}) corresponding to the strongest fragmental contributions. These differences are smoothed with the decrease of molecular packing density. For example, the strongest fragmental interactions for **V** are approximately the same.

The following trends can be observed between the fragmental contributions to the packing energies and molecular van der Waals volumes. As V^{vdw} value increases, the contributions of R_2–R_2 and R_2–R_3 interactions almost do not change, and the contribution of R_2–R_4 interactions reduces, whereas the contributions of R_4–R_5 and R_5–R_5 fragmental interactions grow.

As Figure 4a shows, contributions of intermolecular hydrogen bonds to the packing energy exceed the contributions of the strongest nonbonded van der Waals interactions (except those for **IV**). It is remarkable that for compounds **I**, **II** and **III** similar hydrogen bond networks are observed (two different hydrogen bonds with graph set assignments C(8) and S(6)).[12] However, the hydrogen bond network topology changes essentially with the reduction in the molecular packing density of the crystals. For example, compound **IV** has only one intermolecular hydrogen bond with the energy much less than that of the strongest nonbonded fragmental interactions. The number of hydrogen bonds for **VI** is maximal for the studied substances and equal to three. Moreover, each hydrogen bond (on energy scale) exceeds the fragmental contributions. And finally, substance **V** has two hydrogen bonds, which involve the same molecular fragment; therefore Figure 4a shows only one asterisk. The energies of the hydrogen bonds exceed the fragmental interactions as well.

The next step was to calculate total nonbonding interactions of each molecular fragment with all fragments of adjacent molecules in the crystal lattice. The results of the analysis in $\beta = V^{free}/V^{vdw}$ coordinate scale are presented in Figure 4b. As it was expected, the dominant contribution to the packing energy belongs to R_1, R_2 and R_4. However, the ratio between the contributions changes with the reduction of molecular packing density. For compounds **I** and **II**, having the densest molecular packing, the following regularity is observed: $R_4 > R_1 > R_2$. When the molecular packing density decreases (compounds **III** and **IV**), the relationships take the following form: $R_1 > R_4 > R_2$. Finally, for the less packed substances, **VI** and **V** the regularity $R_1 > R_2 > R_4$ is observed. The contribution of R_5 depends essentially on its size and ability to create hydrogen bonds. For example, if the influence of both of the above-mentioned properties is significant (substance **VI**) the contribution of the R_5 term can be comparable to the dominant inputs R_1, R_2 and R_4. The proposed approach makes it possible

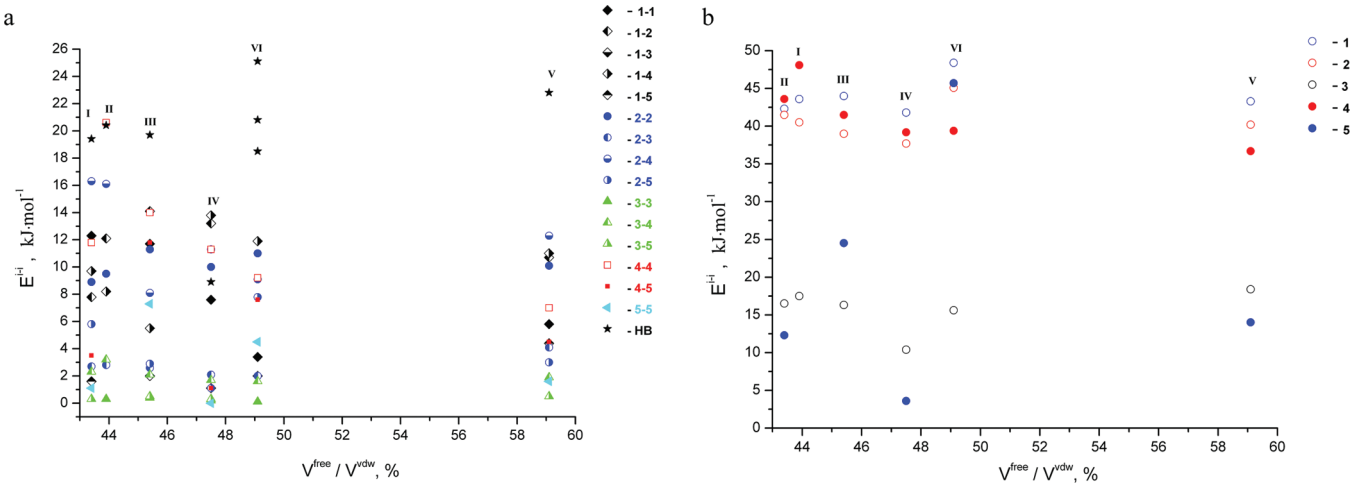

Figure 4. Plot of the contributions of (a) nonbonded van der Waals interactions to the packing energy of different fragment pairs of adjacent molecules (E^{i-i}) and (b) total interactions of each molecular fragment with all fragments of adjacent molecules in the crystal lattice (E^{i-i}) versus V^{free}/V^{vdw} for the studied compounds (asterisks correspond to correction for the hydrogen bond energy).

Table 3. Temperature Dependencies of Saturation Vapor Pressure of the Compounds

IV[a]		V[b]		VI[c]	
t [°C]	$P \times 10^3$ [Pa]	t [°C]	$P \times 10^3$ [Pa]	t [°C]	$P \times 10^3$ [Pa]
75.0	4.89	60.0	4.65	105.0	3.18
76.0	5.63	61.5	5.80	106.5	3.70
77.0	6.35	63.0	7.30	107.5	4.09
78.0	7.08	65.0	9.66	108.0	4.30
79.0	7.83	68.0	16.2	109.0	4.84
80.0	8.65	70.0	22.2	110.0	5.52
82.0	11.7	72.0	30.8	111.0	6.10
83.7	14.6	74.0	46.4	112.0	6.81
85.0	16.6	75.0	53.9	113.0	7.45
87.0	20.7	77.0	78.1	114.0	8.31
89.0	26.3	79.0	98.3	115.5	9.66
90.0	29.3	83.0	163.7	116.0	10.7
91.0	32.4	85.0	223.1	117.0	11.3
92.0	35.8			118.0	12.9
93.0	38.4			119.0	13.8
93.3	41.2			120.0	15.8
95.0	48.3			120.5	16.7
96.0	55.6			121.0	17.8
96.5	56.1			122.0	19.1
97.0	59.0			123.5	23.1

[a] $\ln(P[\text{Pa}]) = (36.9 \pm 0.3) - (14675 \pm 107)/T$; $\sigma = 2.7 \times 10^{-2}$; $r = 0.9995$; $n = 20$. [b] $\ln(P[\text{Pa}]) = (51.3 \pm 0.7) - (18903 \pm 255)/T$; $\sigma = 6.0 \times 10^{-2}$; $r = 0.9985$; $n = 13$. [c] $\ln(P[\text{Pa}]) = (36.6 \pm 0.3) - (16031 \pm 99)/T$; $\sigma = 1.6 \times 10^{-2}$; $r = 0.9996$; $n = 20$.

to analyze the influence of each molecular fragment on the stabilization of crystal lattice energy and opens perspectives for the task-oriented design of drug molecules, assuming, together with optimizing of the molecular solvation energy, the crystal lattice energy minimizing in order to create well water-soluble drugs.

3.2. Sublimation and Thermophysical Characteristics. In order to determine the relationships between the crystal lattice parameters, on one hand, and the sublimation and thermophysical characteristics, on the other hand, we conducted sublimation and DSC experiments. The temperature dependencies of saturated vapor pressure of the considered compounds are summarized in Table 3. The thermodynamic functions of sublimation and fusion processes of the tested compounds are presented in Table 4.

Table 4. Thermodynamic Characteristics of Sublimation and Fusion Processes of the Studied Compounds

	IV	V	VI
ΔG^{298}_{sub} [kJ·mol^{-1}]	59.1	58.6	71.9
ΔH^{T}_{sub} [kJ·mol^{-1}]	122.0 ± 0.9	157 ± 2	133.3 ± 0.8
ΔH^{298}_{sub} [kJ·mol^{-1}]	124.8 ± 0.9	160 ± 2	138.0 ± 0.8
$C^{298}_{p,cr}$ [J·mol^{-1}·K^{-1}][a]	304.4	349.0	348.7
$T\Delta S^{298}_{sub}$ [kJ·mol^{-1}]	65.7	101.4	66.1
ΔS^{298}_{sub} [J·mol^{-1}·K^{-1}]	220 ± 6	339 ± 11	222 ± 8
ς_H [%][b]	65.5	61.2	67.6
ς_{TS} [%][b]	34.5	38.8	32.4
T_m [K]	376.3 ± 0.2	417.2 ± 0.2	418.1 ± 0.2
ΔH^{T}_{fus}[kJ·mol^{-1}]	31.3 ± 0.5	29.9 ± 0.5	43.4 ± 0.5
ΔS^{T}_{fus} [J·mol^{-1}·K^{-1}][c]	83 ± 3	72 ± 3	104 ± 3

[a] $C^{298}_{p,cr}$ has been calculated by additive scheme.[19] [b] $\varsigma_H = (\Delta H^{298}_{sub}/(\Delta H^{298}_{sub} + T\Delta S^{298}_{sub})) \times 100\%$; $\varsigma_{TS} = (T\Delta S^{298}_{sub}/(\Delta H^{298}_{sub} + T\Delta S^{298}_{sub})) \times 100\%$. [c] $\Delta S^{T}_{fus} = \Delta H^{T}_{fus}/T_m$.

The relationship between specific (hydrogen bonding, Coulombic) and nonspecific (van der Waals) interactions in crystal lattice affects the equilibrium solubility value of molecular crystals (drugs). The procedure of splitting the crystal lattice energies into the outlined contributions was reported previously.[28] The nonspecific interactions in crystal lattice, ΔH^{vdw}_{sub}, were estimated by the following equation:

$$\Delta H^{vdw}_{sub} = (11 \pm 2) + (0.46 \pm 0.02)V^{vdw} \quad (18)$$

$$r = 0.973; \sigma = 4.1; n = 71$$

The specific interactions of molecules in the crystal lattice were calculated as a difference between the experimental and

Table 5. Calculated Values of Nonspecific, $\Delta H_{sub}^{nonspec}$, and Specific, ΔH_{sub}^{spec}, Sublimation Enthalpy Terms of the Studied Compounds

compd	V^{vdw} [Å^3]	ΔH_{sub}^{298} [kJ·mol^{-1}]	$\Delta H_{sub}^{nonspec\ a}$ [kJ·mol^{-1}]	$\Delta H_{sub}^{spec\ b}$ [kJ·mol^{-1}]	$\varepsilon_{sub}{}^{c}$ [%]
I[d]	198.8	123.8 ± 1.1	102.4	21.4	20.9
II[d]	214.1	142.0 ± 1.6	109.5	32.5	29.7
III[d]	237.6	152.8 ± 2.2	120.3	32.5	27.0
IV	199.8	124.8 ± 0.9	102.9	21.9	21.3
V	223.7	160 ± 2	113.9	46.1	40.5
VI	236.1	138.0 ± 0.8	119.6	18.4	15.4

[a] Calculated by the correlation equation (18) $\Delta H_{sub}^{nonspec} = \Delta H_{sub}^{vdw}$; statistical error within 4 kJ·mol^{-1}. [b] $\Delta H_{sub}^{spec} = \Delta H_{sub}^{298} - \Delta H_{sub}^{vdw}$. [c] $\varepsilon_{sub} = (\Delta H_{sub}^{spec}/\Delta H_{sub}^{nonspec}) \times 100\%$; experimental error within 6%. [d] Reference 12.

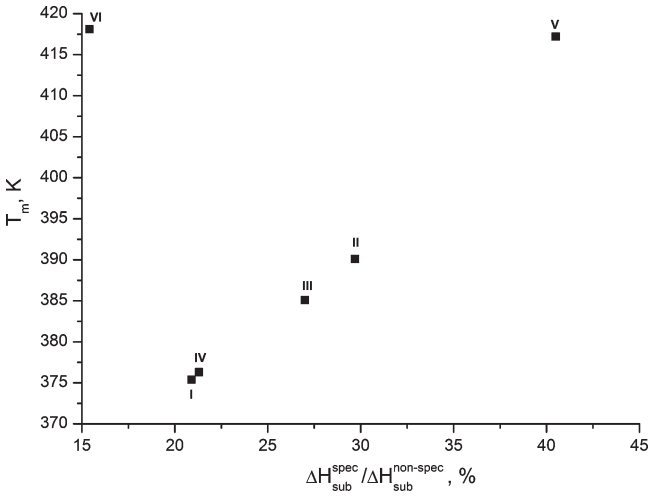

Figure 5. The dependence of melting points versus the ratio between specific and nonspecific molecular interactions ($\Delta H_{sub}^{spec}/\Delta H_{sub}^{nonspec}$) in the crystal lattices of the compounds studied.

nonspecific values. The results of the splitting procedure are summarized in Table 5.

The ratio of specific and nonspecific contributions is defined by the ε_{sub} parameter. According to our previous studies,[12,28] the introduced ε_{sub} parameter correlates with some thermophysical and thermodynamical characteristics. We found similar correlations for the tested compounds. Figure 5 shows experimental data in T_m coordinates versus ε_{sub} parameter. It is evident that a linear trend is observed between the considered variables except those for **VI**. This deviation is difficult to explain, and one of the interpretations of this fact may be connected with the maximal number of hydrogen bonds per molecule (three) in comparison with other compounds.

On the other hand, a linear trend is observed between experimental values ΔG_{sub}^{298} and T_m, except those for **V** (Figure 6a). The reason of this deviation is difficult to explain and it requires accumulation and analysis of additional experimental data. Nevertheless, the two obtained trends give us an opportunity to estimate the absolute value of sublimation thermodynamic characteristics when we know only the melting points. In other words, conducting routine DSC experiments allows us to estimate the sublimation characteristics without time-consuming sublimation experiments.

As the molecular packing in the crystal lattices was determined by various types of interactions, we tried to find out the correlations between ΔG_{sub}^{298} and physicochemical descriptors of program HYBOT.[21] The analysis of 32 descriptors showed that the sublimation Gibbs energy can be best described by the descriptor indicating the sum of H-bond donor−acceptor factors (ΣE_{ad}) of the molecule. The results of the analysis are presented in Figure 6b. It is not difficult to see that the following trend is observed: an increase of ΔG_{sub}^{298} donor−acceptor interactions in crystal structures leads to higher values.

We tried to find out some relationships between the melting points and the fragmental contributions to the packing energies considered in the previous section. The result of the analysis shows that there is a linear trend between the melting points and the contributions from the first and fourth fragments (R_1−R_4): the fusion temperature increases with increase of the interactions between the fragments. This finding means that especially R_1−R_4 fragmental interactions are responsible for the fusion processes of this class of compounds.

3.3. Distribution Processes. Partition coefficients are useful in estimating distribution of drugs within the body. Hydrophobic drugs with high partition coefficients are preferentially distributed to hydrophobic compartments such as lipid bilayers of cells while hydrophilic drugs (low partition coefficients) preferentially are found in hydrophilic compartments such as blood serum. A drug's distribution coefficient strongly affects how easily the drug can reach its intended target in the body, how strong an effect it will have once it reaches its target, and how long it will remain in the body in an active form. In the context of pharmacokinetics the distribution coefficient has a strong influence on ADME properties of the drug. Hence, the hydrophobicity of a compound (as measured by its distribution coefficient) is a major determinant of how druglike it is. Likewise, hydrophobicity plays a major role in determining where drugs are distributed within the body after absorption and as a consequence in how rapidly they are metabolized and excreted.

To describe drug molecules penetration through the blood−brain barrier (BBB) the difference between water/octanol (log P_{oct}) and water/alkane (log P_{alkane}) partition coefficients is usually used as a descriptor.[29] Moreover, cyclohexane (P_{chex}) is applied frequently as an alkane.[8] The log P_{chex} value quantifies the partitioning of the molecule into nonpolar regions of the brain, whereas the log P_{oct} value describes protein interactions in the blood. Thus, in order to optimize the brain penetration of a drug molecule the overall H-bonding property of this molecule has to be minimized. In this work buffer−hexane pair was used as a model barrier to imitate nonspecific (van der Waals) interactions of drug molecules with medium. It should be noted that in some thermochemical studies[30] preference is given to *n*-hexane instead of cyclohexane for estimating of specific and nonspecific

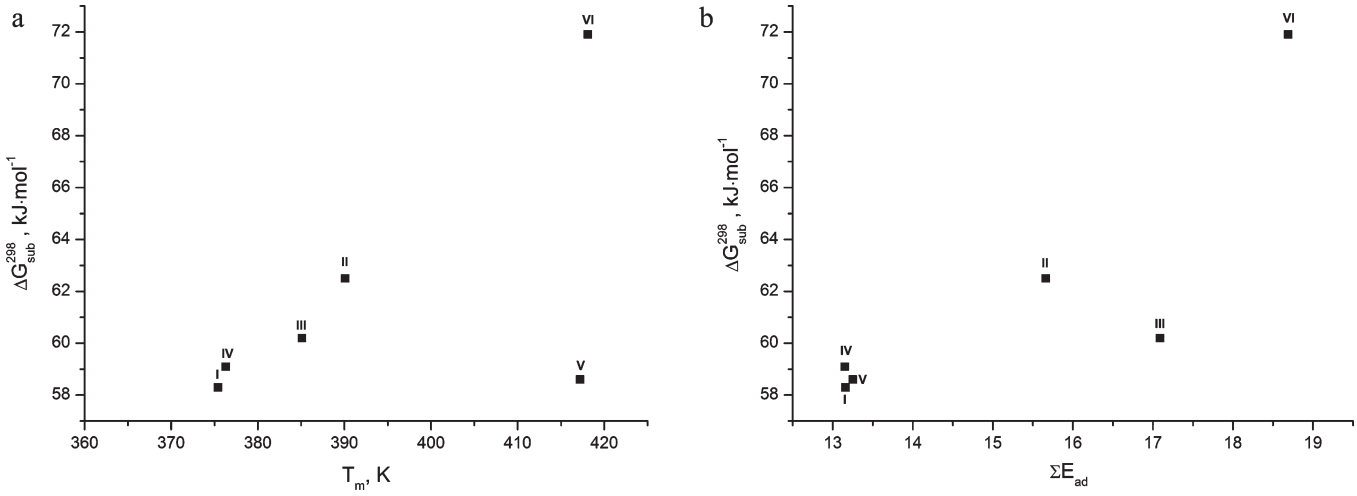

Figure 6. The dependence of sublimation Gibbs energies (ΔG^{298}_{sub}) versus the melting points (a) and the sum of H-bond donor−acceptor factors (ΣE_{ad}) (b) of the tested compounds.

interactions ratio for experimental reasons. As the compounds studied are better soluble in *n*-hexane than cyclohexane, this fact extends the analyzed data set essentially.

We measured the concentration dependence coefficients of distribution at 25 °C in buffer−octanol solutions in order to determine the activity level of the tested compounds in octanol. Figure 7 summarizes these data. As a result, the distribution coefficient of the compound **VI** is not concentration-dependent, whereas compounds **IV** and **V** revealed a weak reduction of the distribution coefficient with the increase of compound concentration in octanol phase (the difference between the studied values exceeds the experimental errors with the number of replications more than three for each concentration). Therefore, at high concentrations of compounds **IV** and **V** in octanol the activity coefficients are different from unity and these coefficients can be assessed by the above-mentioned method as $\gamma_2^o(\mathbf{IV}) \approx D^{7.4\rightarrow oct}_{c(max)}/D^{7.4\rightarrow oct}_{c(min)} = 0.71$, $\gamma_2^o(\mathbf{V}) \approx D^{7.4\rightarrow oct}_{c(max)}/D^{7.4\rightarrow oct}_{c(min)} = 0.63$. The average values of distribution coefficients in buffer−*n*-octanol phase are the following: $D^{7.4\rightarrow oct}(\mathbf{I}) = 149 \pm 36$;[12] $D^{7.4\rightarrow oct}(\mathbf{II}) = 445 \pm 28$;[12] $D^{7.4\rightarrow oct}(\mathbf{III}) = 478 \pm 16$;[12] $D^{7.4\rightarrow oct}(\mathbf{IV}) = 508 \pm 20$; $D^{7.4\rightarrow oct}(\mathbf{V}) = 13327 \pm 77$; $D^{7.4\rightarrow oct}(\mathbf{VI}) = 47 \pm 3$. Since the tested compounds are weakly soluble in *n*-hexane, the distribution coefficients in buffer−*n*-hexane phase are below zero whereas the experimental accuracy is significantly lower than that in the buffer−*n*-octanol system: $D^{7.4\rightarrow hex}(\mathbf{I}) = 0.14 \pm 0.04$;[12] $D^{7.4\rightarrow hex}(\mathbf{II}) = 0.31 \pm 0.05$;[12] $D^{7.4\rightarrow hex}(\mathbf{III}) = 0.12 \pm 0.03$;[12] $D^{7.4\rightarrow hex}(\mathbf{IV}) = 0.32 \pm 0.02$; $D^{7.4\rightarrow hex}(\mathbf{V}) = 0.81 \pm 0.05$; $D^{7.4\rightarrow hex}(\mathbf{VI}) = 0.14 \pm 0.01$. In terms of all of the above-mentioned results, in the buffer−lipophilic (buffer−octanol) solutions all the tested compounds will prefer the lipophilic/transcellular pathways of delivery (octanol phase). In contrast, in order to pass through the BBB (buffer−hexane solutions) all compounds are likely to use the paracellular (aqueous regions) pathways of delivery, as it was shown by Young et al.[8]

3.4. Solubility and Solvation Thermodynamics. The temperature dependencies of the tested compounds solubility in buffer, *n*-hexane and *n*-octanol solutions are summarized in Table 6. The thermodynamic functions of the drug solubility process in the solutions at 298 K are presented in Table 7.

For compounds **II**, **III**[12] and **V** the rank order is similar in the tested solvents, and hence can be arranged in the following order (from most soluble to least soluble): *n*-octanol > *n*-hexane > buffer. In contrast, compounds **I**,[12] **IV**, and **VI** (Table 6 and 7) have a different solubility ranking: *n*-octanol > buffer > *n*-hexane. Moreover, the solubility of compounds in *n*-octanol differs by several orders of magnitude from the solubility in buffer and *n*-hexane. The solubility values for compounds in buffer have the following order (T = 298.15 K): **I** ($X_2 = 9.05 \times 10^{-5}$)[12] > **IV** ($6.13 \times 10^{-5}$) > **II** ($3.95 \times 10^{-5}$)[12] > **V** ($3.09 \times 10^{-6}$) > **III** ($1.79 \times 10^{-5}$)[12] > **VI** ($14.5 \times 10^{-6}$). In *n*-hexane they correspond to the following: **I** ($X_2 = 5.44 \times 10^{-5}$)[12] > **II** ($3.99 \times 10^{-5}$)[12] > **III** ($2.87 \times 10^{-5}$)[12] > **IV** ($2.21 \times 10^{-5}$) > **V** ($1.17 \times 10^{-5}$) > **VI**, whereas for *n*-octanol the order is **IV** ($X_2 = 6.20 \times 10^{-2}$) > **V** ($4.08 \times 10^{-2}$) > **III** ($3.37 \times 10^{-2}$)[12] > **I** ($2.00 \times 10^{-2}$)[12] > **VI** ($9.47 \times 10^{-3}$) > **II** ($7.30 \times 10^{-3}$).[12] The solution enthalpies for the tested compounds in all solvents are positive and have the following order: octanol [**V** (20.5) > **IV** (14.8) ≥ **VI** (14.7)]; buffer [**VI** (50.2) > **V** (25.9) > **IV** (2.7)] and hexane [**V** (42.2) > **IV** (22.2)], which means that the crystal lattice energy overcomes the solvation forces. Entropy values of the solubility of all compounds in *n*-octanol and of **I**, **II**, **III** and **V** compounds in *n*-hexane are positive, whereas for buffer solubility the values of the compounds **I**−**V** are negative. Such a behavior can be explained by the presence of significant hydrophobic effects in these compounds in the examined solvents.

In order to estimate the interaction of compounds with solvents on an absolute energy scale, the solvation thermodynamic functions were calculated for the compounds on the basis of the sublimation and solubility experiments results:

$$\Delta Y^{\circ}_{solv} = \Delta Y^{\circ}_{sol} - \Delta Y^{298}_{sub} \qquad (19)$$

where Y is one of the thermodynamic functions G, H or S.

The thermodynamic functions of solvation processes for the studied compounds in *n*-hexane, buffer and *n*-octanol at 298 K are presented in Table 7. According to the enthalpies of the tested molecules interactions with buffer (absolute values ΔH°_{solv}), they can be arranged in the following order: **V** ($|\Delta H^{\circ}_{solv}| = 133.7$ kJ·mol^{-1}) > **III** (131.4)[12] > **II** (124.9)[12] > **IV** (122.1) > **I** (101.5)[12] > **VI** (87.8). The above order is different for octanol [**V** ($|\Delta H^{\circ}_{solv}| = 139.1$ kJ·mol^{-1}) > **III** (124.8)[12] > **VI** (123.3) > **II** (121.7)[12] > **IV** (110.0) > **I** (95.9)[12]] and hexane (nonspecific interactions) [**V** ($|\Delta H^{\circ}_{solv}| = 117.4$ kJ·mol^{-1}) > **II**

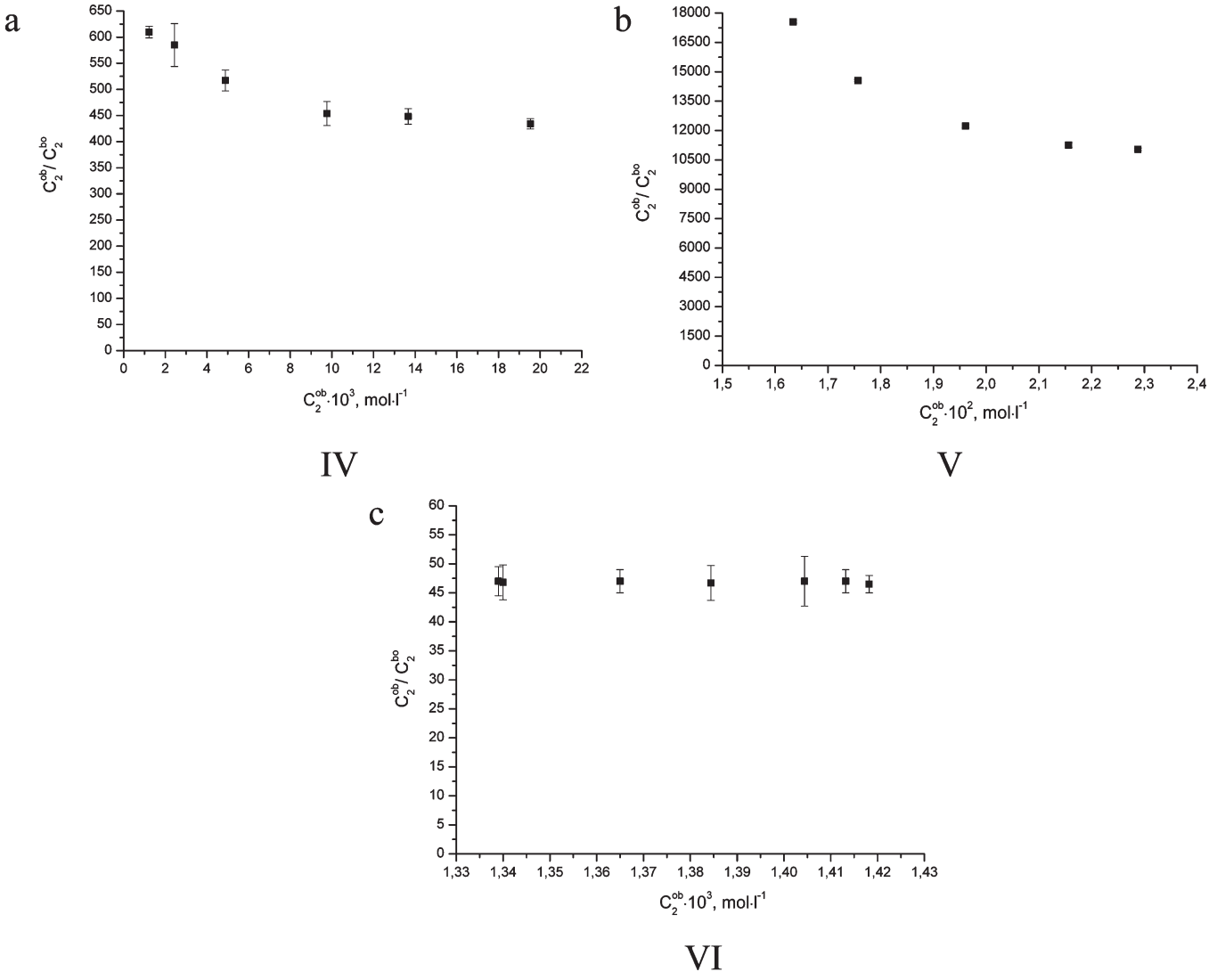

Figure 7. Concentration dependent distribution coefficients of (a) **IV**, (b) **V**, and (c) **VI** compounds in the buffer−*n*-octanol system.

Table 6. The Temperature Dependencies of Solubility, X_2 [mole fraction], of Compounds IV, V and VI in Buffer, *n*-Hexane and *n*-Octanol

	IV			V			VI	
T [K] /t [°C]	buffer: $X_2 \times 10^5$	*n*-hexane: $X_2 \times 10^5$	*n*-octanol: $X_2 \times 10^2$	buffer: $X_2 \times 10^6$	*n*-hexane: $X_2 \times 10^6$	*n*-octanol: $X_2 \times 10^2$	buffer: $X_2 \times 10^5$	*n*-octanol: $X_2 \times 10^3$
293.15/20	6.01	1.90	5.50	2.57	8.72	3.58	1.03	8.63
298.15/25	6.13	2.23	6.33	3.11	11.5	4.08	1.38	9.43
303.15/30	6.13	2.54	6.99	3.62	16.1	4.60	2.15	10.6
310.15/37	6.38	3.10	7.73	4.38	22.1	5.56	3.20	12.1
315.15/42	6.51	3.64	8.16	5.40	29.2	6.46	4.23	13.0
A	−8.6 ± 0.2	−1.8 ± 0.2	3.2 ± 0.3	−2.2 ± 0.3	5.7 ± 0.4	5.1 ± 0.3	9.1 ± 0.9	1.3 ± 0.2
B^a	329 ± 44	2670 ± 68	1780 ± 96	3121 ± 79	5079 ± 125	2468 ± 82	6040 ± 259	1764 ± 55
R^b	0.9740	0.9990	0.9957	0.9990	0.9991	0.9983	0.9973	0.9986
σ^c	8.5×10^{-3}	1.31×10^{-2}	1.84×10^{-2}	1.50×10^{-2}	2.40×10^{-2}	1.60×10^{-2}	4.96×10^{-2}	1.05×10^{-2}

[a] Parameters of the correlation equation: $\ln X_2 = A - B/T$. [b] R: pair correlation coefficient. [c] σ: standard deviation.

$(103.8)^{12}$ > **IV** (102.6) ≥ **III** $(102.3)^{12}$ > **I** $(83.3)^{12}$]. Based on the driving force of solvation (the absolute values of solvation Gibbs energy) all the tested compounds have their own orders for each solvent: for hexane **II** ($|G^{\circ}_{solv}|$ = 37.4 kJ·mol^{-1})^{12} > **III**

dx.doi.org/10.1021/mp2003237 |*Mol. Pharmaceutics* 2011, 8, 1807–1820

Table 7. Thermodynamic Solubility and Solvation Functions of IV, V, VI in *n*-Hexane, Buffer and *n*-Octanol Solutions at 298 K

	X_2	ΔG°_{sol} [kJ·mol^{-1}]	ΔH°_{sol} [kJ·mol^{-1}]	$T\Delta S^\circ_{sol}$ [kJ·mol^{-1}]	ΔS°_{sol} [J·K^{-1}·mol^{-1}]	ΔG°_{solv} [kJ·mol^{-1}]	ΔH°_{solv} [kJ·mol^{-1}]	$T\Delta S^\circ_{solv}$ [kJ·mol^{-1}]	ΔS°_{solv} [J·K^{-1}·mol^{-1}]	ς_{Hsolv}[c] [%]	ς_{TSsolv}[d] [%]
					n-Hexane						
IV	2.21×10^{-5}	26.6	22.2 ± 0.6	−4.4	−15 ± 1	−32.5	−102.6	−70.0	−235	59.4	40.6
V	1.17×10^{-5}	28.2	42.2 ± 0.1	14.0	47 ± 1	−30.4	−117.4	−87.0	−292	57.4	42.6
					Buffer						
IV	6.13×10^{-5}	24.0	2.7 ± 0.4	−21.3	−71 ± 11	−35.1	−122.1	−86.9	−291	58.4	41.6
V	3.09×10^{-6}	31.5	25.9 ± 0.7	−5.6	−19 ± 1	−27.1	−133.7	−106.6	−358	55.6	44.4
VI	14.5×10^{-6}	27.6	50.2 ± 2.1	22.6	76 ± 5	−44.3	−87.8	−43.5	−146	66.9	33.1
					n-Octanol						
IV	6.20×10^{-2}	7.7[a]	14.8 ± 0.8	7.1	24 ± 1	−51.4	−110.0	−58.5	−196	65.3	34.7
V	4.08×10^{-2}	9.1[b]	20.5 ± 0.7	11.1	38 ± 2	−49.5	−139.1	−89.6	−301	60.8	39.2
VI	9.47×10^{-3}	11.6	14.7 ± 0.5	3.1	10 ± 1	−60.3	−123.3	−63.0	−211	66.2	33.8

[a] $\Delta G^\circ_{sol} = -RT\cdot\ln(\gamma_2\cdot X_2)$, where $\gamma_2 = 0.712$ estimated from concentration dependence of distribution experiments. [b] $\Delta G^\circ_{sol} = -RT\cdot\ln(\gamma_2\cdot X_2)$, where $\gamma_2 = 0.629$ estimated from concentration dependence of distribution experiments. [c] $\varsigma_{Hsolv} = [|\Delta H^\circ_{solv}|/(|\Delta H^\circ_{solv}| + |T\Delta S^\circ_{solv}|)] \times 100\%$. [d] $\varsigma_{TSsolv} = [|T\Delta S^\circ_{solv}|/(|\Delta H^\circ_{solv}| + |T\Delta S^\circ_{solv}|)] \times 100\%$.

Table 8. Transfer Thermodynamic Functions of Studied Compounds at 298 K

compd	$-\Delta G^\circ_{tr}$ [kJ·mol^{-1}]	$-\Delta H^\circ_{tr}$ [kJ·mol^{-1}]	$-T\Delta S^\circ_{tr}$ [kJ·mol^{-1}]	$-\Delta S^\circ_{tr}$ [J·mol^{-1}·K]	ε_H[a] [%]	ς_{Htr}[b] [%]	ς_{TStr}[c] [%]
			n-Hexane → Buffer				
IV	2.6	19.5	16.9	56	19.0		
V	−3.3	16.3	19.6	66	13.9		
			n-Hexane → *n*-Octanol				
IV	18.9	7.4	−11.5	−39	7.2		
V	19.1	21.7	2.6	9	18.5		
			Buffer → *n*-Octanol				
IV	16.3	−12.1	−28.4	−95		29.9	70.1
V	22.4	5.4	−17	−57		24.1	75.9
VI	16.0	35.5	19.5	65		64.5	35.5
			Buffer → *n*-Hexane				
IV	−2.6	−19.5	−16.9	−56		53.6	46.4
V	3.3	−16.3	−19.6	−66		45.4	54.6

[a] $\varepsilon_H = (\Delta H_{spec}/\Delta H_{nonspec}) \times 100\%$, where $\Delta H_{spec} = \Delta H_{tr}$(*n*-hexane→solvent) and $\Delta H_{nonspec} = \Delta H^\circ_{solv}$(*n*-hexane). [b] $\varsigma_{Htr} = [\Delta H^\circ_{tr}/(|\Delta H^\circ_{tr}| + |T\Delta S^\circ_{tr}|)] \times 100\%$. [c] $\varsigma_{TStr} = [T\Delta S^\circ_{tr}/(|\Delta H^\circ_{tr}| + |T\Delta S^\circ_{tr}|)] \times 100\%$.

(34.3)[12] ≥ **I** (34.0)[12] > **IV** (32.5) > **V** (30.4); for buffer solution **VI** ($|G^\circ_{solv}|$ = 44.3 kJ·mol^{-1}) > **II** (37.4)[12] > **I** (35.2)[12] ≥ **IV** (35.1) > **III** (33.1)[12] > **V** (27.1); and finally for octanol **VI** ($|G^\circ_{solv}|$ = 60.3 kJ·mol^{-1}) > **IV** (51.4) = **III** (51.4)[12] > **II** (50.3)[12] > **V** (49.5) > **I** (48.6)[12]. The Gibbs energy of the tested compounds solvation in hexane and buffer solution differs slightly, but in octanol the driving forces vary by more than 10 kJ·mol^{-1}.

In the same way as for the intermolecular interactions for crystals, we divided interactions in solutions into specific and nonspecific components. As a measure of nonspecific interactions of soluble molecules with the solvent we selected the thermodynamic functions of solvation in *n*-hexane where van der Waals interactions prevail. In their turn, the specific interactions correspond to the difference between the thermodynamic functions of solvation in current solvent (*n*-octanol or buffer) and *n*-hexane (Table 8). In order to compare the enthalpy values of specific and nonspecific interactions in solutions we introduced the following parameter:

$$\varepsilon_H = (\Delta H_{spec}/\Delta H_{nonspec})\cdot 100\% = [\Delta H^\circ_{solv}(\text{solvent}) - \Delta H^\circ_{solv}(n\text{-hexane})]/\Delta H^\circ_{solv}(n\text{-hexane}) \times 100\% \quad (20)$$

For convenience of performing the analysis of correlation of specific components to nonspecific interactions in buffer and *n*-octanol solutions we derived the following parameters (Figure 8a). Similar properties for solvents and crystals are compared in Figure 8b. Figure 8a shows that for compounds **I**−**IV** the ε_H parameter for buffer solutions exceeds the corresponding value for octanol solutions, and for compound **V** there is an opposite trend. Specifically, for buffer solutions the values are ε_H(**III**) = 28.4%[12] > ε_H(**I**) = 21.8%[12] > ε_H(**II**) = 20.3%[12] > ε_H(**IV**) = 19.0% > ε_H(**V**) = 13.9%, whereas for *n*-octanol: ε_H(**III**) = 22.0%[12] > ε_H(**V**) = 18.5% > ε_H(**II**) = 17.2%[12] > ε_H(**I**) = 15.1%[12] ε_H(**IV**) = 7.2%. It is likely that specific interactions in buffer solution for compounds **I**−**IV** predominate over the octanol solution due to better interaction with small water molecules compared to bulky octanol, facilitating full H-bonding. However, the electrostatic interaction may play a role in contributing to the specific interaction component. It is rather important to compare the thermodynamic parameters of transfers from hexane to octanol phase. Such hypothetical transfer contributes to our understanding of different thermodynamic states of the molecules in a medium that may be a model for BBB (*n*-hexane) and a medium that mimics gastrointestinal epithelium cell membranes (octanol). In all cases the transfer takes place into the octanol phase (negative Gibbs energy), due to specific interactions of the molecules with the solvent. The order of the driving force of this process is the following (in order of decrease): $|\Delta G^{h\to o}_{tr}(\mathbf{V})|$ = 19.1 > $|\Delta G^{h\to o}_{tr}(\mathbf{IV})|$ = 19.0 > $|\Delta G^{h\to o}_{tr}(\mathbf{III})|$ = 17.1[12] > $|\Delta G^{h\to o}_{tr}(\mathbf{I})|$ = 14.6[12] > $|\Delta G^{h\to o}_{tr}(\mathbf{II})|$ = 12.9 kJ·mol^{-1}.[12] During the transfer of compounds **I** and **IV** the entropy of the system increases, i.e. the transfer of molecule from hexane to octanol facilitates disordering of octanol phase. In contrast, a similar process for compounds **II**, **III** and **IV** leads to an entropy decrease and as a result to increased order of lipophilic phase. As

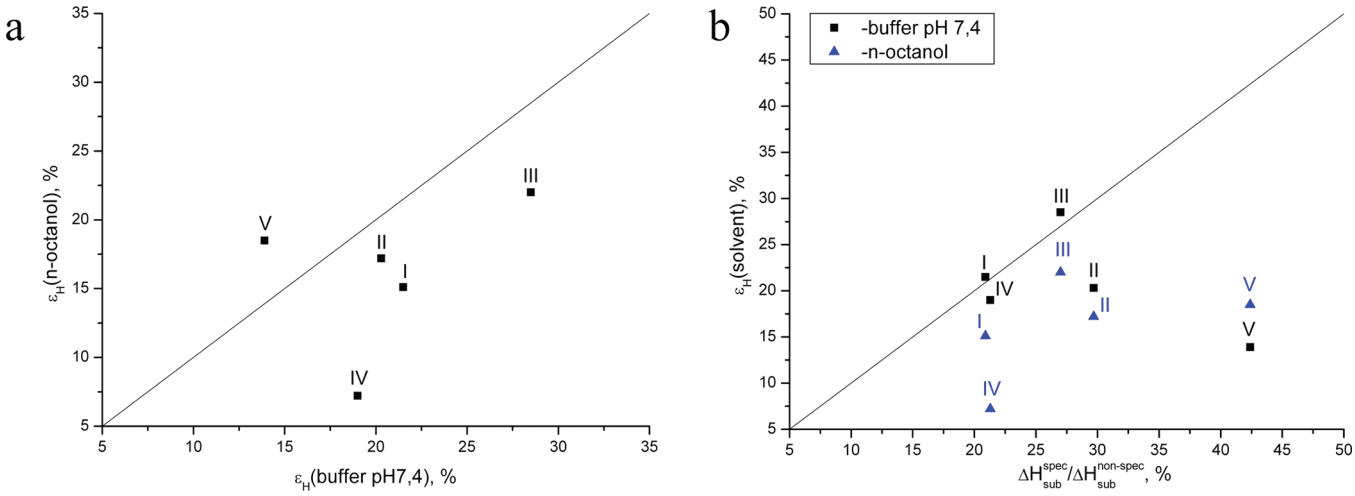

Figure 8. Relationships between (a) the ε_H(*n*-octanol) values for *n*-octanol versus the ε_H(buffer) values for the buffer; (b) the ε_H(solvent) values for the considered solvents versus the ratio between specific and nonspecific enthalpic terms in crystal lattices for the compounds studied. The straight line corresponds to bisector.

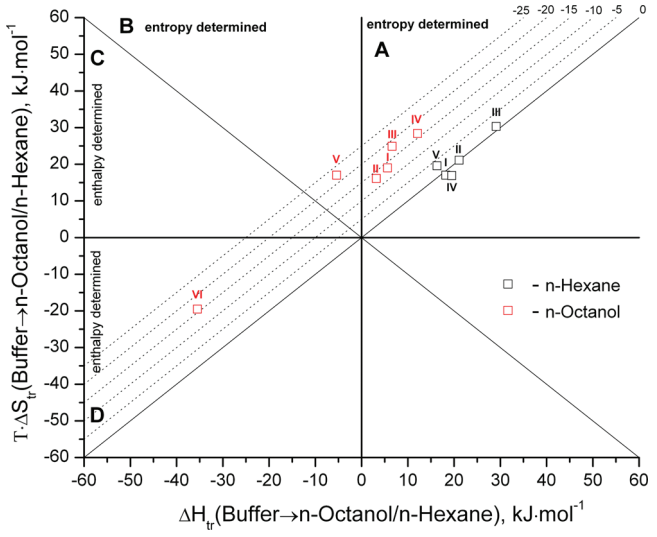

Figure 9. Relationship between the enthalpic and entropic terms of the buffer/*n*-hexane to *n*-octanol transfer functions (see text for numbering of the compounds). The isoenergetic curves of the ΔG_{tr}° function are marked by dotted lines.

it was mentioned above, to describe drug brain penetration (in particular for characteristic log(C_{brain}/C_{blood}) values) the difference between log P_{oct} and log P_{alkane} is usually used. In our case this descriptor can be depicted as a transfer of Gibbs energy from *n*-hexane to *n*-octanol. Young et al.[8] observed an inversely proportional dependence between log(C_{brain}/C_{blood}) and Δ log *P*: with an increase in Δ log *P* the value log(C_{brain}/C_{blood}) decreases. The analysis of $\Delta G_{tr}^{n\rightarrow o}$ values taken into account, it can be assumed that the most favorable conditions for the brain penetration are those of compound **II**, whereas less favorable conditions are those of **V**.

The comparison of ε_H parameters for solutions and crystals is summarized in Figure 8b. The bisecting line corresponds to identical ε_H values for both solutions and crystals. Compounds **I** and **III** have the same ε_H values (within experimental error) in aqueous buffer solution as in the crystal, i.e. all H-bonds are also formed in the buffer. Interestingly, this is not the case for compounds **II**, **IV** and **V**. For all compounds in octanol not all the H-bonds are formed due to steric hindrance as outlined above (Figure 8a,b). However, in crystals due to a very dense packing of molecules all H-bonding partners are fulfilled to a full extent and can be set as an upper margin of ε_H-parameter for such solvents as buffer and octanol.

3.5. Thermodynamics of Molecular Transfer Processes from the Buffer to *n*-Hexane/*n*-Octanol. The thermodynamic transfer functions from the buffers to *n*-octanol/*n*-hexane mixture for the studied compounds were obtained in view of reflecting some biopharmaceutical properties of drugs (Table 8). The experimental data of the thermodynamic functions of the tested compounds are collected in Figure 9. The regions where ($T\Delta S_{tr}^{\circ} > \Delta H_{tr}^{\circ} > 0$) $\equiv$ sector **A** and ($\Delta H_{tr}^{\circ} < 0$; $T\Delta S_{tr}^{\circ} > 0$; $|T\Delta S_{tr}^{\circ}| > |\Delta H_{tr}^{\circ}|$) $\equiv$ sector **B** correspond to the entropy determined processes. The regions of the diagram where ($\Delta H_{tr}^{\circ} < 0$; $T\Delta S_{tr}^{\circ} > 0$; $|\Delta H_{tr}^{\circ}| > |T\Delta S_{tr}^{\circ}|$) $\equiv$ sector **C** and ($\Delta H_{tr}^{\circ} < 0$; $T\Delta S_{tr}^{\circ} < 0$; $|\Delta H_{tr}^{\circ}| > |T\Delta S_{tr}^{\circ}|$) $\equiv$ sector **D** correspond to the enthalpy determined processes. Isoenergetic curves of the ΔG_{tr}° function are marked as dotted lines in Figure 9.

Both analyzing the chemical potentials differences of the transfer processes from water to *n*-octanol phases and comparing the enthalpic and entropic terms of these processes is a useful approach to understand (a) the size of a substructure unit which takes part in the partitioning process and (b) the driving forces of the outlined processes. For example, if the transfer enthalpy is positive, we assume that the drug molecule interactions are stronger with the solvate shell in the water phase than with the octanol phase. Moreover, the equilibrium solubility value of water in the *n*-octanol phase is 2.5 mol·L^{-1}. In this case the substructure of the transferring unit is likely a drug molecule plus a solvation shell. At $\Delta H_{tr}^{\circ} < 0$ we observed the opposite effect: nearly complete resolvation of the drug molecule in water phase during the transferring process. Thus, the substructure of the transferring unit is simply a drug molecule. The entropic term shows that the system ordering changes while the substructure unit is transferred from one phase to another. Thus, first, sector **A** corresponds to the transfer (of drug plus the solvation shell)

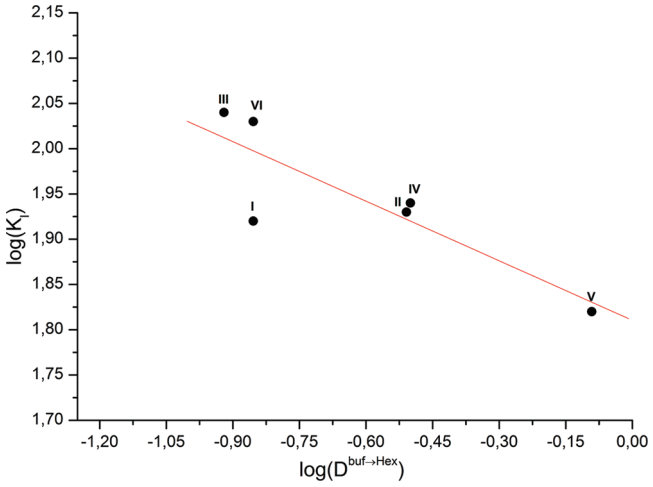

Figure 10. Relationship between the ability to inhibit Glu-Ca uptake ($\log K_I$) and the distribution coefficients in buffer/hexane system ($D^{buf \rightarrow hex}$).

from water to octanol phases with essential disordering of the latter. Second, sector **B** corresponds to the transfer of an individual drug molecule with essential disordering of octanol phase. Third, sector **C** corresponds to the transfer of an individual drug molecule with inessential disordering of the octanol phase. Finally, sector **D** corresponds to transfer of an individual drug molecule with the octanol phase ordering. This information can be useful to analyze the drug molecule's diffusion through biological barriers (passive transport) as the size of the substructure unit plays the key role in this process and determines the mechanism and coefficient values of the diffusion.

It is rather obvious that the transfer processes for the studied compounds have different behavior for substitutes of different nature. The buffer/*n*-octanol transfer process for compounds **I**−**IV** with H− (**I**), CH_3− (**II**), C_2H_5O− (**III**), and F− (**IV**) substituents in the para position is determined by the entropy with a positive value of the transfer enthalpies. This combination of thermodynamic function of the transfer processes is ideal for diffusion of molecules in the lipophilic medium (passive transport) in contrast to other examined sectors of the diagrams. First, the drug molecule interacts weakly with the lipophilic medium as compared to water phase. Second, during the processes of transfer (distribution) of molecules from the water phase to the lipophilic medium, the entropy increases, which corresponds to the increase in structure imperfection (free volume) of the lipophilic phase compared to the water phase. The availability of some space and weak interactions with the surrounding medium contributes to less stringent diffusion of the dissolved molecules in the concentration gradient. As a result, these compounds have the maximum driving force of transfer. Introduction of the substitute for F_3C− in the molecule's para position (compound **V**) leads to a small increase in the distribution coefficient and shifting the meaning for compound **V** from sector **A** to **B** (the enthalpic number sign of compound **V** is negative). CH_3−CHOH− introduction does not change the Gibbs energy, but compound **VI** is located in sector **D** and the distribution process for this compound is determined by enthalpy. So, the CH_3−CHOH− introduction changes the number sign of the thermodynamic functions and, therefore, the driving forces of the transfer process.

Essentially the experimental values of thermodynamic functions of the transfer process from buffer to hexane for the compounds are positioned along or near the bisector with values of driving force near zero. This would mean that there is no driving force for the transition between the aqueous phase and hexane, in other words, for overcoming the blood−brain barrier.

So, the present study confirms the strategy for drug discovery, represented in our previous paper. It means that not only the pharmacological effect (receptor binding activity) but also optimized biopharmaceutical properties enable the compounds to overcome biological barriers. As a result, compounds **I**−**IV**, placed in sector **A** of the diagram (Figure 9), and among them compound **III** with Gibbs energy of transfer at a maximum (distance to bisector) can be chosen in the capacity of most reliable drug molecules with optimal passive transport properties.

3.6. Calcium-Blocking Property Experiments. The results of the tested compounds for their ability to inhibit Glu-Ca uptake are the following: K_I(**III**) = 110 ± 10% > K_I(**VI**) = 108 ± 8% > K_I(**IV**) = 88 ± 16% ≥ K_I(**II**) = 85 ± 4% ≥ K_I(**I**) = 83 ± 6% > K_I(**V**) = 66 ± 13%. We tried to find out correlations between the biological activity values and the measured distribution coefficients of buffer/octanol and buffer/hexane systems. A trend is observed between $\log(K_I)$ and $\log(D^{buf \rightarrow hex})$ (Figure 10): with growth of the distribution coefficient $D^{buf \rightarrow hex}$ the biological activity increases. Thus, it can be assumed that, at the selected model for study of ability to inhibit Glu-Ca uptake, passive transport through the BBB barrier is a limiting stage of the drug delivery process.

4. CONCLUSION

The three new crystal structures of the 1,2,4-thiadiazoles have been solved by X-ray diffraction experiments. The packing architecture and hydrogen bond networks were analyzed by graph set notations and compared with analogous compounds published by us earlier. The thermodynamic aspects of the 1,2,4-thiadiazole sublimation processes were studied on the basis of temperature dependencies of vapor pressure by means of transpiration method. We defined specific and nonspecific contributions of molecular interactions in the crystal and introduced the ε_{sub} parameter, which describes the ratio of these two values. We found that the introduced parameters correlate with melting temperatures. On the other hand, the melting points correlate with sublimation Gibbs energies. The sublimation Gibbs energy can be best described by the descriptor indicating the sum of H-bond donor−acceptor factors of the molecule: an increase of donor−acceptor interactions in crystal structures leads to higher ΔG_{sub}^{298} values. We tried to find out some relationships between the melting points and the fragmental contributions to the packing energies. There is a linear trend between the melting points and the contributions from the first and fourth fragments (R_1−R_4): the fusion temperature increases with increase of the interactions between the fragments. This finding means that especially R_1−R_4 fragmental interactions are responsible for the fusion processes of this class of compounds.

The thermodynamic functions of solubility and solvation processes were analyzed using temperature dependencies of solubility in buffer, *n*-hexane and *n*-octanol as well as sublimation characteristics of the tested compounds. We also analyzed specific and nonspecific interactions of the tested compounds with solvents. The obtained values were compared with analogous parameters in crystals. The concentration dependence of

selected compounds was determined in buffer/*n*-octanol at 25 °C, and activity coefficients of molecules in octanol phase were analyzed as well. In addition, we examined the distribution processes of molecules in buffer/*n*-octanol and buffer/*n*-hexane systems. The transfer processes were studied by using the diagram method with analysis of enthalpic and entropic terms. Also, using our analysis it was possible to distinguish between enthalpy and entropy contributions, which led us to more insights that each term is distinct for different molecules (entropy- or enthalpy-determined).

Calcium-blocking properties of tested compounds were also determined. A trend is observed between $\log(K_I)$ and $\log(D^{buf\rightarrow hex})$: with growth of the distribution coefficient $D^{buf\rightarrow hex}$ the biological activity increases.

AUTHOR INFORMATION

Corresponding Author

*Russian Academy of Sciences, Institute of Solution Chemistry, Akademucheskaia, 1, 153045 Ivanovo, Russian Federation. Tel: +7 4932 533784. Fax: +7 4932 336237. E-mail: glp@isc-ras.ru.

ACKNOWLEDGMENT

The present research was funded as part of the basic research programs established by the Presidium of the Russian Academy of Sciences "Fundamental Sciences for Medicine" and "Medical and Biomolecular Chemistry". This work was supported by the Russian Foundation for Basic Research (Project No.09-03-00057).

REFERENCES

(1) Martínez, A.; Alonso, M.; Castro, A.; Pérez, C.; Moreno, F. J. First non-ATP competitive glycogen synthase kinase 3 β (GSK-3β) inhibitors: Thiadiazolidinones (TDZD) as potential drugs for the treatment of Alzheimer's disease. *J. Med. Chem.* **2002**, *45*, 1292–1299.

(2) Martínez, A.; Alonso, M.; Castro, A.; Arán, V. J.; Cardelus, I.; Baños, J. E.; Badía, A. Synthesis and potential muscarinic receptor binding and antioxidant properties of 3-(thiazolyl)pyridine 1-oxide compounds. *Arch. Pharm. (Weinheim, Ger.)* **1999**, *332*, 191–194.

(3) Martínez, A.; Fernández, E.; Castro, A.; Conde, S.; Rodríguez-Franco, I.; Baño, J. E.; Badía, A. E. N-Benzylpiperidine derivatives of 1,2,4-thiadiazolidinone as new acetylcholinesterase inhibitors. *Eur. J. Med. Chem.* **2000**, *35*, 913–922.

(4) Macleod, A. M.; Baker, R.; Freedman, S. B.; Patel, S.; Merchant, K. J.; Roe, M.; Saunders, J. Synthesis and muscarinic activities of 1,2,4-Thiadiazoles. *J. Med. Chem.* **1990**, *33*, 2052–2059.

(5) Alonso, M.; Martínez, A. GSK-3 inhibitors: discoveries and developments. *Curr. Med. Chem.* **2004**, *11*, 753–761.

(6) Lanzafame, A.; Christopoulos, A. Investigation of the interaction of a putative allosteric modulator, N-(2,3-Diphenyl-1,2,4-thiadiazole-5-(2H)-ylidene) methanamine hydrobromide (SCH-202676), with M_1 muscarinic acetylcholine receptors. *J. Pharmacol. Exp. Ther.* **2004**, *308*, 830–837.

(7) Hansch, C.; Bjorkroth, J. P.; Leo, A. Hydrophobicity and central nervous system agents: On the principle of minimal hydrophobicity in drug design. *J. Pharm. Sci.* **1987**, *76*, 663–686.

(8) Young, R. C.; Mitchell, R. C.; Brown, T. H.; Ganellin, C. R.; Griffiths, R.; Jones, M.; Rana, K. K.; Saunders, D.; Smith, I. R.; Sore, N. E.; Wilks, T. J. Development of a new physicochemical model for brain penetration and its application to the design of centrally acting H2 receptor histamine antagonists. *J. Med. Chem.* **1988**, *31*, 656–671.

(9) Abraham, M. H.; Chadha, H. S.; Mitchell, R. C. Hydrogen bonding. 33. Factors that influence the distribution of solutes between blood and brain. *J. Pharm. Sci.* **1994**, *83*, 1257–1268.

(10) Abraham, M. H.; Chadha, H. S.; Mitchell, R. C. Hydrogen bonding. Part 36. Determination of blood brain distribution using octanol-water partition coefficients. *Drug Des. Discovery* **1995**, *13*, 123–131.

(11) Abraham, M. H.; Chadha, H. S. Applications of a solvation equation to drug transport properties. In *Lipophilicity in Drug Action and Toxicology*; Pliska, V., Testa, B., van de Waterbeemd, H., Eds.; Methods and Principles in Medicinal Chemistry, Vol. 4; VCH Publishers: Weinheim, 1995.

(12) Perlovich, G. L.; Volkova, T. V.; Proshin, A. N.; Sergeev, D. Yu.; Bui, C. T.; Petrova, L. N.; Bachurin, S. O. Synthesis, pharmacology, crystal properties and quantitative solvation studies from a drug transport perspective for three new 1,2,4-thiadiazoles. *J. Pharm. Sci.* **2010**, *99* (9), 3754–3768.

(13) Lazarev, A. I.; Kharlamov, I. P.; Yakovlev, P. Y.; Yakovleva, E. F. Hand-book of chem-analyst; Metallurgiya: Moscow, 1976; pp 132−135.

(14) Enraf-Nonius. *CAD-4 Software*, Version 5.0; Enraf-Nonius: Delft, The Netherlands, 1989.

(15) Sheldrick, G. M. *SHELXL97 and SHELXS97*; University of Göttingen: Germany, 1997.

(16) Perlovich, G. L.; Bauer-Brandl, A. Solvation of drugs as a key for understanding partitioning and passive transport exemplified by NSAIDs. *Curr. Drug Delivery* **2004**, *1* (3), 213–226.

(17) Zielenkiewicz, W.; Perlovich, G.; Wszelaka-Rylik, M. The vapour pressure and the enthalpy of sublimation determination by inert gas flow method. *J. Therm. Anal. Calorim.* **1999**, *57*, 225–234.

(18) Cox, J. D.; Pilcher, G. *Thermochemistry of organic and organometallic compounds*; Academic Press: London, 1970.

(19) Chickos, J. S.; Acree, W. E., Jr. Enthalpies of sublimation of organic and organometallic compounds. 1910−2001. *J. Phys. Chem. Ref. Data* **2002**, *31* (2), 537–698.

(20) Pascual-Ahuir, J. L.; Silla, E. GEPOL: An improved description of molecular surfaces. I. Building the spherical surface set. *J. Comput. Chem.* **1990**, *11*, 1047.

(21) Raevsky, O. A.; Grigor'ev, V. J.; Trepalin, S. V. HYBOT program package, Registration by Russian State Patent Agency N 990090 of 26.02.99.

(22) Gavezzotti, A.; Filippini, G. Chapter 3. Energetic aspects of crystal packing: Experiment and computer simulations. In *Theoretical aspects and computer modeling of the molecular solid state*; Gavezzotti, A., Eds.; John Wiley & Sons: Chichester, 1997; pp 61−97.

(23) Mayo, S. L.; Olafson, B. D.; Goddard, W. A., III. Dreiding: A generic force field for molecular simulations. *J. Phys. Chem.* **1990**, *94*, 8897–8909.

(24) Vivona, N.; Cusmano, G.; Macaluso, G. Mononuclear heterocyclic rearrangements. Part 11. Rearrangements of 1,2,4-oxadiazoles, isoxazoles, and 1,2,5-oxadiazoles involving a sulphur atom. *J. Chem. Soc., Perkin Trans. 1* **1977**, 1616–1619.

(25) Etter, M. C. Encoding and decoding hydrogen-bond patterns of organic compounds. *Acc. Chem. Res.* **1990**, *23*, 120–126.

(26) Bernstein, J.; Davis, R. E.; Shimoni, L.; Chang, N.-L. Patterns in Hydrogen Bonding: Functionality and Graph Set Analysis in Crystals. *Angew. Chem., Int. Ed. Engl.* **1995**, *34* (15), 1555–1573.

(27) Perlovich, G. L.; Ryzhakov, A. M.; Tkachev, V. V.; Hansen, L. Kr. Sulfonamide Molecular Crystals: Thermodynamic and Structural Aspects. *Cryst. Growth Des.* **2011**, *11*, 1067–1081.

(28) Perlovich, G. L.; Volkova, T. V.; Manin, A. N.; Bauer-Brandl, A. Influence of position and size of substituents on the mechanism of partitioning: a thermodynamic study on acetaminophens, hydroxybenzoic acids, and parabens. *AAPS PharmSciTech* **2008**, *9* (1), 205–216.

(29) Seiler, P. Interconversion of Lipophilicities from Hydrocarbon/water Systems into the Octanol/Water System. *Eur. J. Med. Chem.* **1974**, *9*, 473–479.

(30) Toulmin, A. J.; Wood, M.; Kenny, P. W. Toward Prediction of Alkane/Water Partition Coefficients. *J. Med. Chem.* **2008**, *51*, 3720–3730.